Characterization of EV/HEV NVH issues using electrical machine tooth FRF

K. Degrendele [1], **J. Le Besnerais** [1], **R. Pile** [1,2,3], **P. Gning** [1], **E. Devillers** [1]
[1] EOMYS ENGINEERING,
Lille Hellemmes, France
e-mail: **contact@eomys.com**

[2] Univ. Lille, Arts et Métiers ParisTech, Centrale Lille, HEI, EA 2697
L2EP -Laboratoire d'Electrotechnique et d'Electronique de Puissance,
F-59000 Lille, France

[3] Univ. Artois, EA 4025, Laboratoire Systèmes Electrotechniques et Environnement (LSEE),
F-62400 Béthune, France

Abstract
This article extends the use of tooth Frequency Response Functions (FRF) concept for the analysis of electric motor Noise, Vibration and Harshness due to electromagnetic forces (e-NVH) at intermediate design stage or after manufacturing, using both simulation and testing. The principle consists in first characterizing the structural response of the housing envelope when exciting stator teeth under harmonic loads. Then tooth FRF can be converted to wave FRF to analyze the structural response under rotating Maxwell stress waves. These wave FRF can be used for modal parameter extraction, or to study the effect of eccentricities by modulating pulsating magnetic forces driving the NVH behavior of e-motors in electric and hybrid electric vehicles (EV / HEV) automotive applications. Besides, tooth FRF can be used to visualize the operational magnetic force waves acting on the stator using Operational Force Shape analysis. Longitudinal FRF concept is also introduced to study skewing effects and optimize the skewing pattern combining tests with simulation under MANATEE software, specialized on the electromagnetic and vibroacoustic design of electric motors. Finally, the extension of the concept on stator FRF to rotor FRF is discussed.

1 Introduction

Magnetic forces in electrical machines are a significant source of Noise, Vibration and Harshness (NVH), which can be responsible of high tonal noise. Multi-physics modeling including electric, electromagnetic, structural and acoustic calculations is performed to predict noise levels at a design stage.

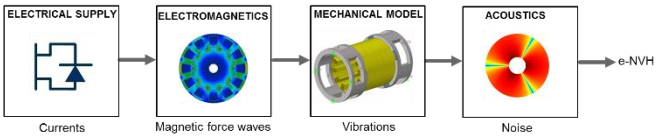

Figure 1: Multi-physics modeling for noise and vibration assertion in e-machines [1]

Magnetic forces can be distinguished by their respective frequency and spatial distribution along the airgap of the electrical machine. The spatial distribution frequency is called circumferential wavenumber and noted *r*. Some examples of force circumferential wavenumbers are given in Figure 2.

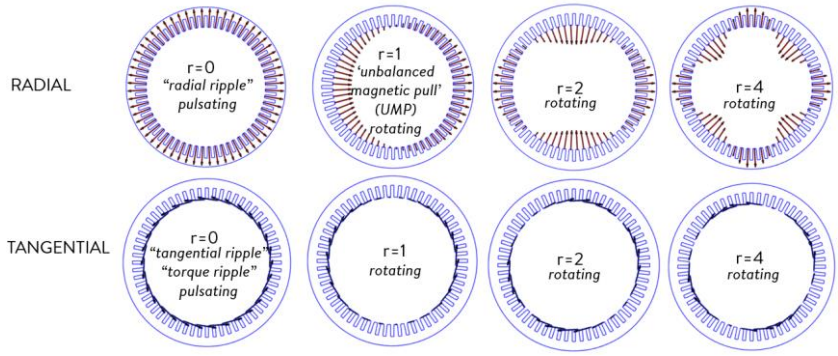

Figure 2. Examples of rotating or pulsating Maxwell stress waves along the electrical machine circumference (r = 0: pulsating, r = 1: UMP)

r = 0 corresponds to a pulsating vibration wave; r = 1 to an Unbalanced Magnetic Pull (UMP), the magnetic equivalence of a mechanical imbalance; other magnetic force harmonics always rotate.

Each of the above Maxwell stress wave induces magnetic radial and tangential forces on each tooth's tip numerated with $i \in [1, Z_s]$ as in (1) and (2) according to [1,2]:

$$F_{rad_{r,i}}(\omega) = RL\frac{2}{r}\sin\left(r\frac{\pi}{Z_s}\right)\sigma_{rad}\,(r,\omega)e^{jr\alpha_i} \quad (1)$$

$$F_{tan_{r,i}}(\omega) = RL\frac{2}{r}\sin\left(r\frac{\pi}{Z_s}\right)\sigma_{tan}\,(r,\omega)e^{jr\alpha_i} \quad (2)$$

where:

- R: stator bore radius [m],
- L: stator stack length [m],
- r: circumferential wavenumber [NA],
- Z_s: number of stator teeth [NA],
- σ_{rad} : Maxwell radial stress wave [N/m²],
- σ_{tan} : Maxwell tangential stress wave [N/m²],
- i: node on a stator tooth tip [NA],
- αi: angular tooth position [rad].

The summation of individual forces for each wavenumber corresponds to the total magnetic force applied on each tooth's tip *i*:

$$F_{rad_i}(\omega) = \sum_r F_{rad_{r,i}}(\omega) \quad (3)$$

$$F_{tan_i}(\omega) = \sum_r F_{tan_{r,i}}(\omega) \quad (4)$$

This paper is presenting a complementary approach to full e-NVH virtual prototyping. Indeed, a mechanical numerical model always requires to be fitted with experiments (e.g. using Experimental Modal Analysis) due to complex electrical motor material properties (e.g. winding, orthotropic laminations), unknown damping and uncertain boundary conditions (e.g. frame to stator shrink fit, weldings).

If a prototype is manufactured, modal basis characterization might not be the most convenient way to quantify the structural behavior of the stator and frame assembly under magnetic excitations. Experimental Modal Analysis characterizes all structural modes, even the ones which cannot be excited by magnetic forces due to mismatch between magnetic force shape and modal shape.

This new approach aims at assessing the contribution of individual electromagnetic excitation harmonics to the overall vibration or Sound Power Level of the machine. Then the physical origin of the key excitation contributors is provided allowing to speed up the diagnosis and the choice of noise mitigation strategies.

This paper first describes the concept of a tooth FRF including its measurement and simulation methodologies. Then the conversion method from tooth FRF to wave FRF, which gives physical insights to the results, is detailed.

Finally, the importance of wave FRF to identify the root cause of e-NVH harmonics is highlighted. An application case is included through all the sections.

2 Stator tooth FRF

2.1 General principle

A tooth FRF consists in loading a specific stator tooth with an impulse force while monitoring the structural response of the stator housing external envelope. Excitation is either radial or tangential leading to respectively a radial or a tangential tooth FRF.

2.2 Experimental protocol

An impact hammer and accelerometers are used to characterize stator tooth FRF by tests, to respectively apply the excitation and measure its effect on the structure.

Applying a hammer shock excitation on a stator tooth's tip (force on point *i*) is often unfeasible due to limited space. Alternatively, it is possible to apply the excitation on the external envelope of the stator (force on node *k*) in normal direction while monitoring the structural response of a certain stator tooth (velocity on node *i*). This assumes that the reciprocity principle [3] holds, implying the following equivalences:

$$FRF_{rad_{k,i}} = FRF_{rad_{i,k}} \tag{5}$$

$$FRF_{tan_{k,i}} = FRF_{tan_{i,k}} \tag{6}$$

for which *k* is a point on the stator external envelope and *i* a point on a tooth's tip. Figure 3 illustrates each side if the equations (5) and (6).

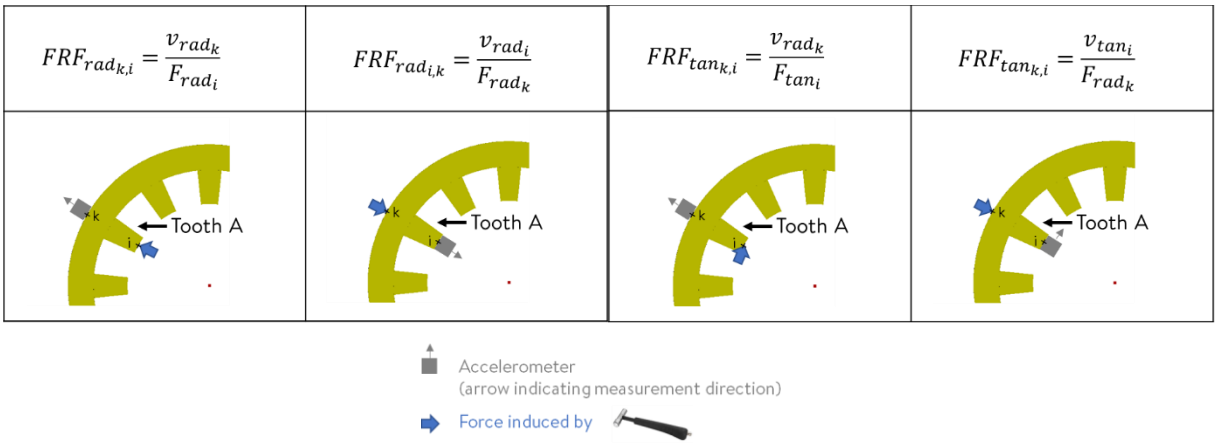

Figure 3. Measurement test set-ups for radial tooth FRF (top) and tangential tooth FRF (bottom)

2.3 Simulation

Characterizing stator Tooth FRF can also be performed numerically using FEA (Finite Element Analysis). Several models are built to model experimental conditions with loading impulse forces.

2.4 Application

Measurements and simulations are both performed on a benchmark machine specifically designed to illustrate the interaction between magnetic forces and the structural response of electrical machines [4], [5], [6]. The geometrical of the studied stator is presented in Figure 4.

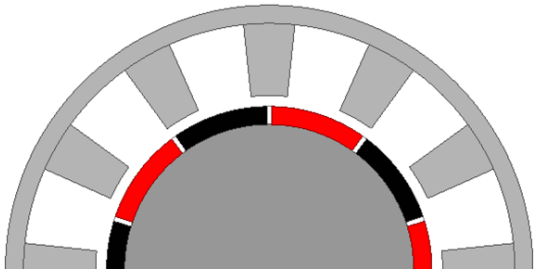

Figure 4. 12S10P SPMSM benchmark machine [4]

Experiments are done using twelve 3D accelerometers glued on each tooth's tip in successively four different planes as described on Figure 5 and Figure 6. Both radial and tangential accelerations are monitored while successively impacting the 96 points of the external stator envelope. All measurements are carried with OROS OR38 32 channel and OR35 10 channel acquisition systems.

This is leading to 9216 (96 times 12 times 4 times 2) different tooth FRF, half radial and half tangential. Examples of radial stator tooth FRF are given in Figure 7 for the first measurement plane.

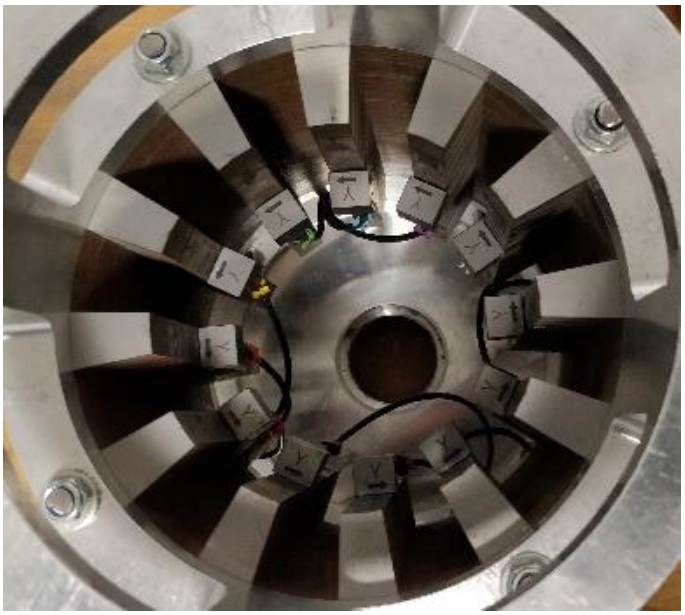

Figure 5. 12S10P benchmark stator equipped with 12 3D accelerometers

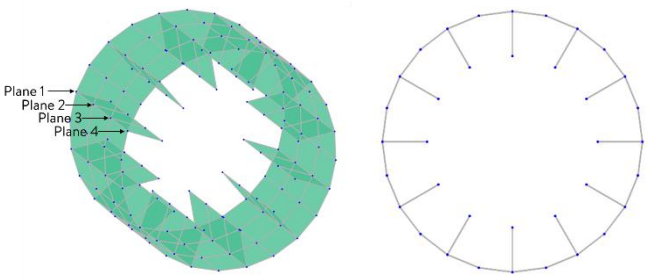

Figure 6. Experimental mesh implemented on 12S10P benchmark machine for stator tooth FRF (4 planes of 24 points externally, 4 planes of 12 points internally)

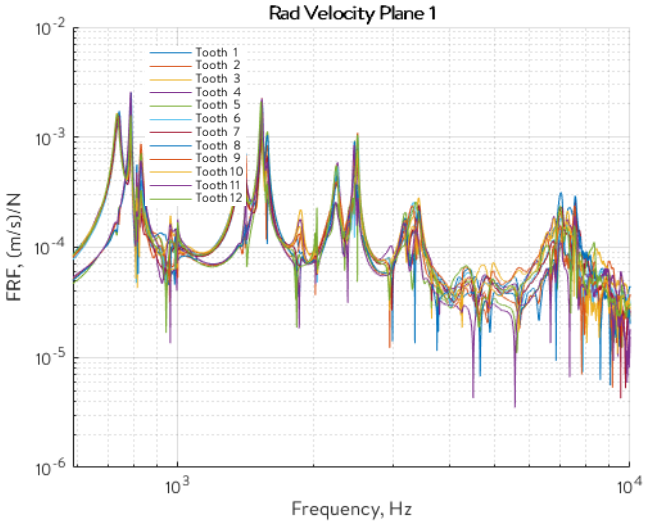

Figure 7. Average radial stator tooth FRF when impacting on node 1 to 96 while measuring on nodes 97 to 108 (plane 1)

The validity of the reciprocity principle has been checked by measurement in radial direction (refer to Figure 8). It still needs to be validated in tangential direction using a dedicated stator with significant space between teeth to allow access for a tangential hammer's hit.

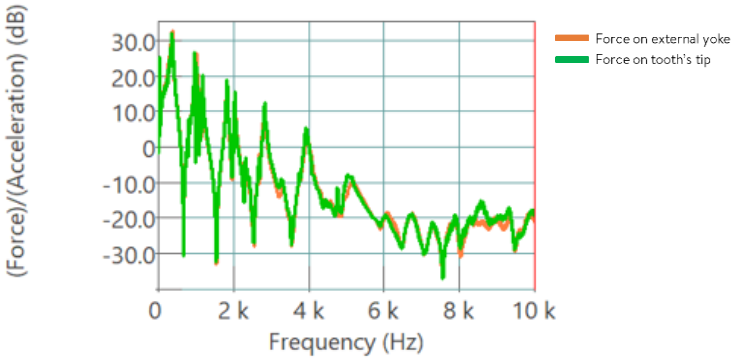

Figure 8. Stator tooth FRF when impacting on node 50 while measuring on node 121, and vice versa

3 Stator Circumferential Wave FRF

3.1 General principle

Once all stator Tooth FRF are acquired (either by simulation or by test), a specific computation is applied to analyze the local structural response of electric machine under rotating Maxwell stress waves of circumferential wavenumber *r*. For each node on the external stator envelope *k*:

$$WFRF_{rad_{r,k}} = RL\frac{2}{r}sin\left(r\frac{\pi}{Z_s}\right)\sum_{i=1}^{i=Z_s} FRF_{rad_{k,i}}(\omega)\, e^{jr\alpha_i} \tag{7}$$

This formula has been validated in [2] for a given plane.

Similarly:

$$WFRF_{tan_{r,k}} = RL\frac{2}{r}\sin\left(r\frac{\pi}{Z_s}\right)\sum_{i=1}^{i=Z_s} FRF_{tan_{k,i}}(\omega)\, e^{jr\alpha_i} \tag{8}$$

3.2 Specifities

Maxwell stress waves with high wavenumbers are usually neglected. However recent work [7] shows that they must be considered and that they can easily be assessed. Indeed, Maxwell stress waves of wavenumbers $r+uZ_s$ are folded back into Maxwell stress waves of wavenumbers *r* (with *u*: integer) due to tooth sampling. Analytically, it can be shown that WFRF integrates this effect as:

$$WFRF_{rad_{r+uZ_s,k}} = WFRF_{rad_{r,k}} \tag{9}$$

Besides, analytically the following equation holds:

$$WFRF_{rad_{-r,k}} = WFRF_{rad_{r,k}} \tag{10}$$

which is valid for axisymmetric systems. Otherwise, system structural response amplitudes are different when excited by a stress wave of wavenumber *r* than when excited by a stress wave of wavenumber *-r*. They depend on system boundary conditions.

3.3 Application

Radial and tangential circumferential wave FRF are derived using (7) and (8) then RMS values are assessed as per (11) where n_e is the total number of nodes on the external stator envelope. Results shown in Figure 9 are similar in both directions apart from ~ 4000Hz. It is linked to the measurement quality of tangential tooth FRF above 4000Hz. Indeed, the tooth FRF coherence function which quantifies how much the accelerometer signal is related to the hammer signal is further away from one from ~ 4000Hz, meaning lower measurement quality.

$$WFRF_{rad_{r,RMS}} = \sqrt{\frac{1}{n_e}\sum_{k=1}^{n_e} abs\left(WFRF_{rad_{r,k}}{}^2\right)} \tag{11}$$

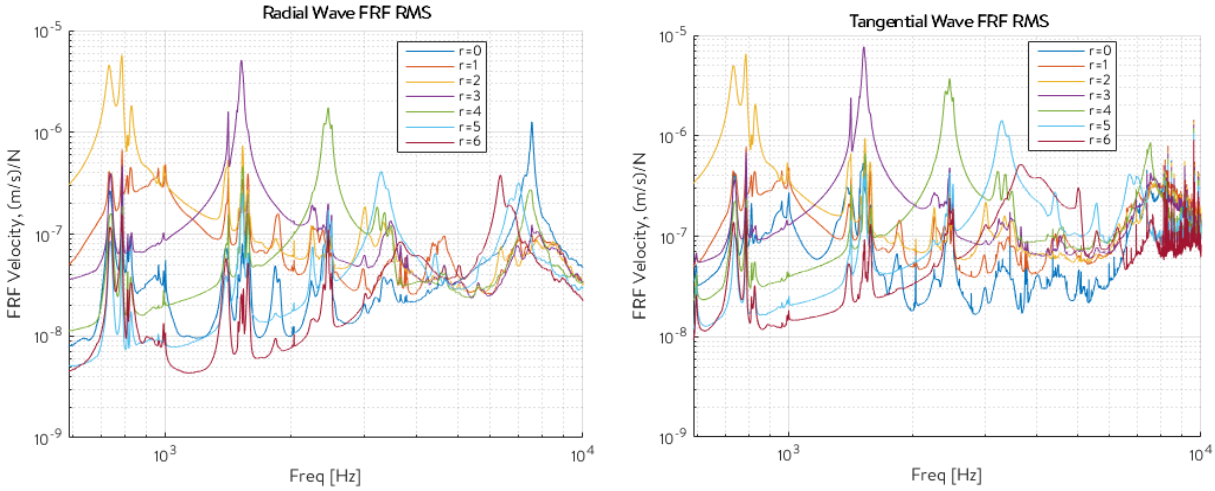

Figure 9. Radial (top) and tangential (bottom) stator circumferential Wave FRF RMS

4 Stator longitudinal Wave FRF

4.1 General principle

In addition to the circumferential wavenumber *r*, a longitudinal wave number *s* must be introduced when having variation of magnetic stress along the machine length (case of skewing). It refers to the spatial frequency of a magnetic stress wave in the axial direction. An example is given in Figure 10 to illustrate a magnetic stress wave of $r = 2$ and $s = 1$.

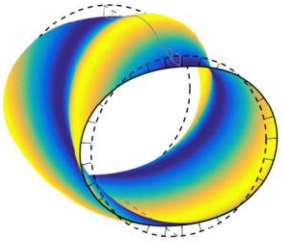

Figure 10. Radial stress wave ($r = 2$, $s = 1$)

As tooth FRF can be measured (or calculated) on different planes, longitudinal WFRF can as well be extracted. If the teeth are continuous in the longitudinal direction, an arbitrary number N_p of longitudinal stator tooth tip node (or experimental impact points) can be chosen. Using the same mathematical framework from [8], the integrated load applying on a longitudinal section *p* can be expressed as:

$$F_{rad_{s,k}}(\omega) = \frac{2L}{s\,\pi} sin\left(\frac{s\pi\Delta L}{L}\right) \sigma_{rad}(s,\omega).\, e^{js\pi L_p} \tag{12}$$

Then the longitudinal wave FRF response of a tooth *i* at a point *k* on the yoke on a longitudinal section *p* can be calculated:

$$WFRF_{rad_{s,k}} = \frac{2L}{s\,\pi} sin\left(\frac{s\pi\Delta L}{L}\right) \sum_{i=1}^{i=N_p} FRF_{rad_{k,i}}(\omega)\, e^{js\pi L_p} \tag{13}$$

Where:

- s: longitudinal wavenumber [NA],
- ΔL: half-length between two consecutive excitation points [m],
- Lp: relative length (between 0 and 1) of each tooth tip longitudinal node.

Rotor or stator skewing induces axial forces on the electrical machine. Longitudinal WFRF are key to quantify the effects and optimize the skewing pattern combining tests with simulation under MANATEE software.

4.2 Application

Radial longitudinal wave FRF is derived using formula 7 and 12 then RMS value is assessed. Results are presented in Figure 11.

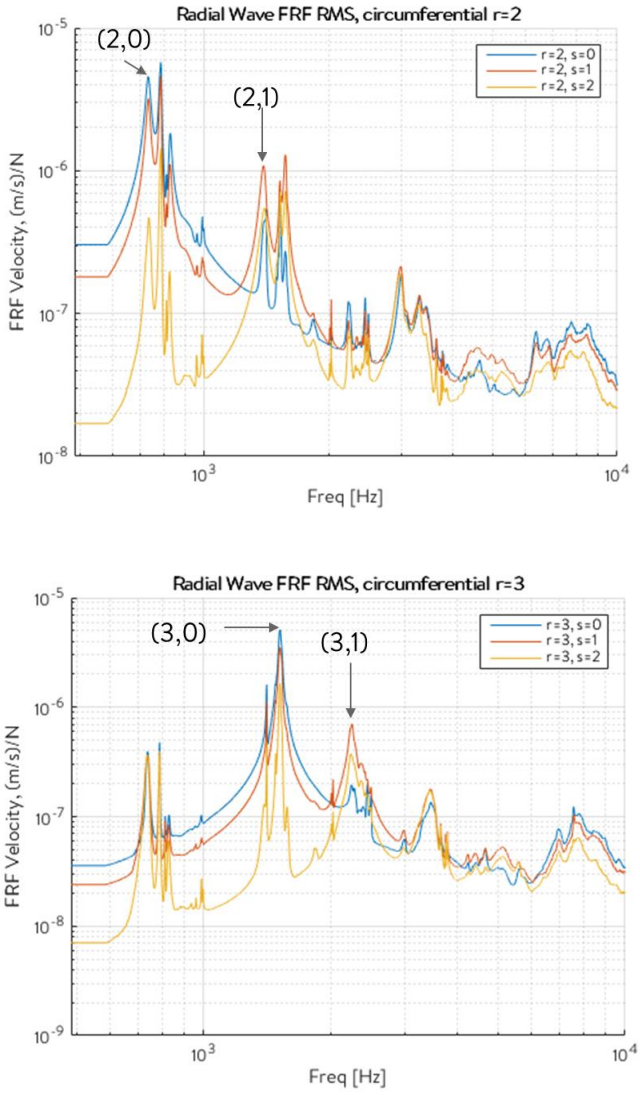

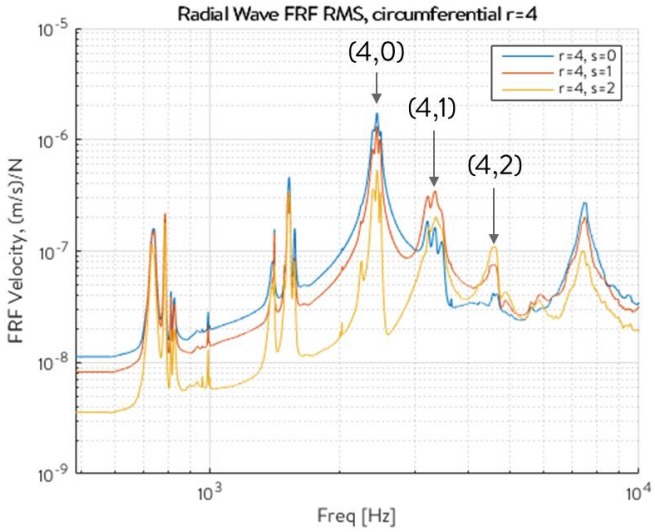

Figure 11. Radial stator Wave FRF RMS for *r*=2,3 and 4, *s*=0,1 and 2

5 Key outputs with application

Stator WFRF allows to analyze the response of the electric machine under specific rotating Maxwell stress waves.

5.1 Key contributions

Based on the amplitude of each magnetic excitation harmonics associated to a given wavenumber (from the electromagnetic step from **Error! Reference source not found.**), it is possible to identify the key contributors to the overall vibration and overall acoustic power of the machine.

First, the velocity of each external node *k* is computed based on the excitation of each magnetic harmonic, associated to a pulsation and wavenumber r:

$$\underline{v}_k = \sum_r \underline{v}_{r,k} = \sum_r WFRF_{rad_{r,k}} F_{rad,r} + WFRF_{tan_{r,k}} F_{tan,r} \tag{14}$$

where WFRF can be reconstructed from measured tooth FRF or simulated on FEA software, magnetic excitations harmonics F are generally generated from electromagnetic simulation as the airgap electromagnetic flux density is difficult to capture experimentally, ω is the pulsation frequency.

Then, the square of the RMS velocity v_{RMS}^2 of the machine external surface is calculated using:

$$v_{RMS}^2 = \frac{1}{S}\iint_S (\underline{v}.\underline{v}^*).dS = \frac{1}{n_t}\sum_{k=1}^{n_e} \underline{v}_k.\underline{v}_k{}^* \tag{15}$$

with S the external surface of the machine, $\underline{\boldsymbol{v}}$ the complex velocity of an elementary oriented surface $\boldsymbol{dS}$, which turns into a discrete summation if all elementary surfaces are identical, n_e the number of nodes on the external stator envelope.

Finally machine acoustic power W can be characterized from the square of the RMS velocity of its external surface using:

$$W(\omega) = \frac{1}{2}\rho c S \sigma v_{RMS}^2 \tag{16}$$

where ρ is air mass density, c is sound velocity in air, σ is the acoustic radiation factor.

Assuming unit radiation factor (as per Equivalent Radiation Power), one can therefore obtain an image of Sound Power Level under each Maxwell stress wave.

Having extracted both $WFRF_{rad_{r,k}}$ and $WFRF_{tan_{r,k}}$, it is possible to conclude on the contribution of the tangential forces to the overall displacement.

5.2 Modal parameters

Plotting displacement WFRF for several wavenumbers allows to identify modal shapes, natural frequencies and modal damping of the studied structure. It assumes representative boundary conditions while characterizing tooth FRF.
Natural frequencies can be captured by extracting the peak-value for each wavenumber. Modal damping can be extracted based on the width of the peak as described in Figure 12.

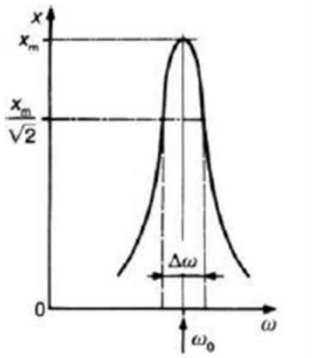

$$\frac{\Delta\omega}{\omega_0} = 2\varepsilon$$

Figure 12. Damping extraction process based on displacement FRF

A comparison with modal parameters obtained by Experimental Modal Analysis (EMA) is given in Table 1.

Natural frequencies are accurately captured with a maximum of 8% deviation. However, damping deviation is significant, apart from breathing mode which is at 2%. The reason for the damping discrepancies needs to be further investigated.

Table 1: Modal parameter comparison between EMA and radial displacement WFRF

Mode number	WFRF frequency (Hz)	EMA frequency (Hz)	Natural frequency deviation (%)	WFRF damping (%)	EMA Damping (%)	Damping deviation (%)
(0,0)	7542	7583	-1	0.6	0.6	2
(2,0)	731	741	-1	1.3	0.5	147
(3,0)	1517	1532	-1	0.9	0.5	77
(4,0)	2450	2474	-1	1.0	0.5	117
(5,0)	3283	3450	-5	2.2	0.8	182
(6,0)	3659	3968	-8	5.2	0.8	567
(2,1)	1391	1394	0	1.5	1.1	30
(3,1)	2248	2262	-1	1.5	1.2	19
(4,1)	3345	3314	1	2.4	1.5	58
(5,1)	4400	4356	1	2.5	0.9	185
(4,2)	4619	4580	1	2.7	2.0	30
(5,2)	5566	5618	-1	1.9	1.8	9

5.3 Effect of asymmetries

Dummy sets of tooth FRF can be built based on a single tooth measurement to study the effect of stator asymmetry. The dummy set linked to a tooth T_i assumes all the other teeth have the same response function relatively to their position. In particular, a dummy set for tooth T5 can be calculated based on tooth T1 assuming:

$$FRF_{rad_{N6,T5}} = FRF_{rad_{N22,T1}} \tag{17}$$

and equivalent relationships for the other nodes and tooth.

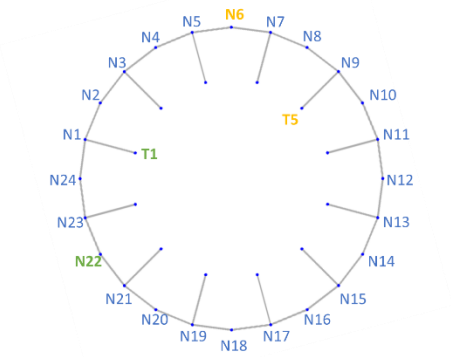

Figure 13. Stator section showing nodes on the external envelope and tooth numbers.

Dummy sets of WFRF can then be derived. Figure 14 compares dummy WFRF of wavenumber r = 2 calculated based on tooth n°1, with the one based on tooth n°2. Original WFRF of wavenumber r = 2 integrating all teeth measurements is overlaid as a reference. The ear located in front of tooth n°2 (refer to Figure 15) is reducing the amplitude of the structural response due to an excitation of wavenumber 2 around 720Hz.

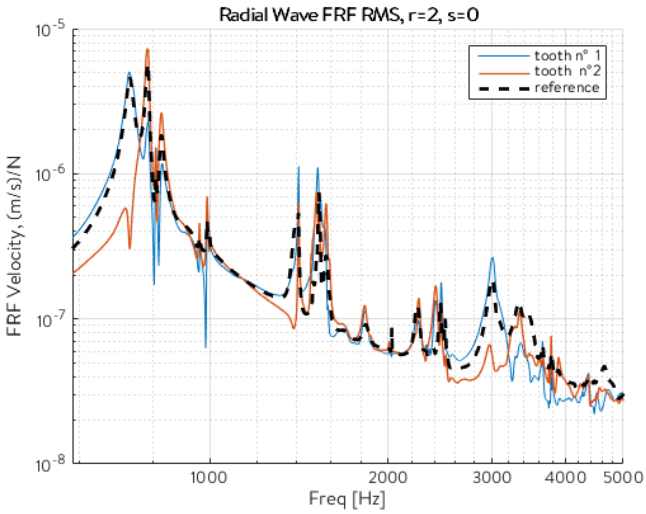

Figure 14. WFRF of wavenumber r=2 based on dummy sets linked to tooth n°1 and tooth n°2 and the reference integrating all teeth measurements

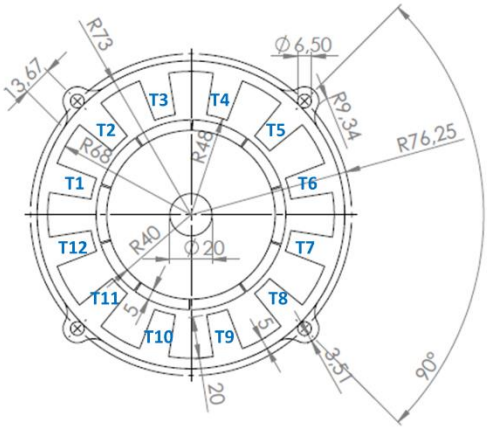

Figure 15. Stator section showing ears in front of tooth n°2, tooth n°5, tooth n°8 and tooth n°11.

5.4 Effect of eccentricities and uneven airgap

Both eccentricities and uneven airgap lead to Unbalanced Magnetic Pull (UMP) forces of wavenumber 1 (or -1). Knowing WFRF associated to a wavenumber 1 (and -1), it is possible to account for a force amplitude increase of UMP and quantify its impact on the overall displacement of the structure, and then to the noise radiated by the structure.

Indeed, assuming force amplitude being proportional to the square of flux density and flux density being proportional to the inverse of the airgap, a small eccentricity of ε% in the airgap creates additional forces of wavenumbers r +/- 1 with an amplitude 2ε % of F as illustrated on Figure 16.

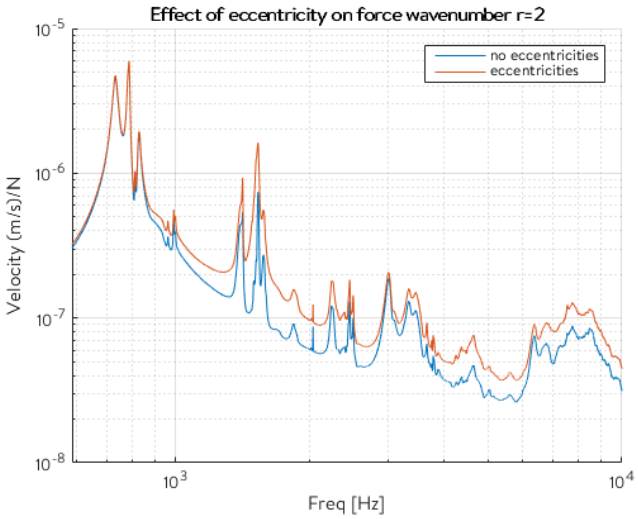

Figure 16. Effect of 10% of eccentricity on a force r=2 of 1N amplitude

6 Possible extensions

6.1 Operational Magnetic Force Shapes

An Operational Magnetic Force Shape (OFS) consists in visualizing the operational magnetic force shape at a certain frequency and a certain speed. As for an Operational Deflection Shape (ODS), an OFS requires to monitor the displacement of the stator external envelope while the structure is being excited by its internal

operational forces. Additionally, tooth FRF as defined in (1) and (2) are needed to reconstruct both radial and tangential forces on each tooth node *i* using the following formula [9]:

$$F_{rad_i} = FRF_{rad_{k,i}}^{-1} d_{rad_k} \quad (18)$$

$$F_{tan_i} = FRF_{tan_{k,i}}^{-1} d_{rad_k} \quad (19)$$

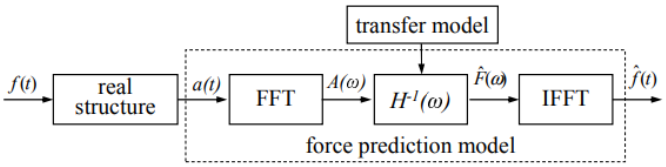

Figure 17. Direct force prediction method.

When an OFS is carried around the e-motor stator at a frequency where driving forces are mainly of electromagnetic origin, one can visually analyze the nature of the force excitation (rotating or pulsing) and the rotation direction. An OFS can also confirm the main wavenumber of a radial or tangential force excitation.

Besides, the maximum circumferential wavenumber that can be captured with an OFS corresponds to the number of stator teeth divided by two, assuming 1 node per stator tooth's tip per plane is defined, and according to Shannon theorem (e.g. on a stator with 12 teeth, 12 accelerometers are used to capture a maximum circumferential wavenumber = 6).

6.2 Rotor FRF

Radial force waves of wavenumber $r > 1$ and $r = 0$ applied to an inner rotor do not create significant deflections due to high shaft stiffness. However radial force wave of wavenumber $r = 1$ generate bending of the rotor shaft. Measurement of stator FRF $r = 1$ does not include the excitation of rotor bending mode. Future work therefore aims at deriving UMP rotor FRF separately for more accuracy.

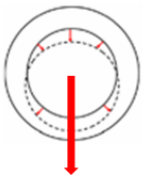

Figure 18. Rotor shaft bending

To investigate further the contribution of the radial magnetic force $r = 1$ on structure borne noise through rotor shaft vibration, the concept of stator tooth FRF can be extended to rotor tooth FRF. Acceleration could be monitored on both bearings while successively impacting the rotor on different points.

7 Conclusions

This paper presents a measurement technique based on stator tooth Frequency Response Function post processing to more directly capture the airborne e-NVH behaviour of electric motor stators. Tooth FRF based on impact hammer measurements are converted into Maxwell pressure wave FRF.

This method can be used to accurately optimize the mechanical integration of the stator into the frame, without carrying any electromagnetic calculations. For instance, it can be used to estimate the sound pressure level variations among several stator to frame coupling techniques, or several impregnation techniques, under specific magnetic force patterns such as UMP, torque ripple or radial ripple.

Alternatively, this method can be used to carry fast and accurate e-NVH design optimization after stator manufacturing on any design variable that does not affect stator FRF: rotor magnetic circuit design (e.g. pole shaping, skewing pattern optimization) and e-motor control (e.g. current angle, commutation strategy, harmonic current injection). As an example, such FRF can be imported in MANATEE software specialized in electrical drives NVH simulation.

Finally, further developments are planned on the indirect visualization of operational magnetic stress waves and rotor FRF to provide additional tools for e-NVH troubleshooting.

8 References

[1] W. Liang, "The investigation of electromagnetic radial force and associated vibration in permanent magnet synchronous machines," in *PhD. dissertation*, Cranfield University, 2017.

[2] R. Pile, J. Le Besnerais, K. Degrendele, "e-NVH Response Synthesis of Electric Motors Based on Stator Teeth FRF Measurements", *ISEF*, 2019.

[3] P. Avitabile, "Experimental modal analysis," *Sound and vibration*, vol. 35, no. 1, pp. 20–31, 2001.

[4] Eomys Engineering, "e-NVH benchmark", 2018. [Online]. Available: *https://eomys.com/recherche/article/e-nvh-benchmark.*

[5] E. Devillers, M. Hecquet, X. Cimetière, J.-P. Lecointe, J. Le Besnerais and T. Lubin, "Experimental benchmark for magnetic noise and vibrations analysis in electrical machines," in *2018 XIII International Conference on Electrical Machines (ICEM)*, pp. 745–751, 2018.

[6] E. Devillers, "Electromagnetic subdomain modeling technique for the fast prediction of radial and circumferential stress harmonics in electrical machines," *PhD*, 2018.

[7] H. Fang, D. Li, R. Qu, P. Yan, "Modulation Effect of Slotted Structure on Vibration Response" in *Electrical Machines IEEE Transactions on Industrial Electronics*, IEEE, 66, 2998-3007, 2019.

[8] MANATEE, "Magnetic Acoustic Noise Analysis Tool for Electrical Engineering," [Online]. Available: *www.manatee-software.com*, 2020.

[9] Oosterhuis, E. J., "Force Prediction via the inverse FRF using experimental and numerical data from a demonstrator with tuneable nonlinearities", 2006.

A. Definitions/Abbreviations

FRF	Frequency Response Function
NVH	Noise, Vibration, Harshness
ODS	Operational Deflection Shape
OFS	Operational Force Shape
r	Circumferential wavenumber
s	Longitudinal wavenumber
σ	Stress
WFRF	Wave Frequency Response Function
Zs	Number of stator teeth